Materials Transactions, Vol. 48, No. 7 (2007) pp. 1717 to 1721
Special Issue on Bulk Metallic Glasses —Selected Papers from the Fifth International Conference on Bulk Metallic Glasses (BMGV)

Thermal Stability and Mechanical Properties of Spray-Formed and Melt-Spun $Al_{89}La_6Ni_5$ Metallic Glass Matrix Composites

M.-L. Ted Guo[1], Chi Y. A. Tsao[1,*], K. F. Chang[1], J. C. Huang[2] and J. S. C. Jang[3]

[1]*Department of Materials Science and Engineering, and Frontier Material and Micro/Nano Science and Technology Center, National Cheng Kung University, 1 Da-Shieh Rd., Tainan, Taiwan, R.O. China*
[2]*Institute of Materials Science and Engineering, National Sun Yat-Sen University, 70 Lien-Hai Rd., Kaohsiung, Taiwan, R.O. China*
[3]*Department of Materials Science and Engineering, I-Shou University, Section 1, Hsueh-Cheng Rd., Ta-Hsu Hsiang, Kaohsiung Country, Taiwan, R.O. China*

A spray-formed $Al_{89}La_6Ni_5$ metallic glass matrix composite plate was obtained in thickness of 1 mm and diameter of 200 mm, comprising over 64% primary crystals (*e.g.* $Al_{11}La_3$) uniformly dispersed in the glass matrix. The microstructure can not be achieved by annealing corresponding amorphous precursor. The crystals existing in the glass matrix were found to increase the hardness of the composite. Through nanoindentation test, the hardness and modulus of the composite at ambient temperature were found superior than its amorphous ribbon counterpart. The hardness of the composite was estimated with the rule of mixture from the constituents to be 4.4 GPa, which agreed well with the nanoindentation results. From loss modulus measurement and TMA test at elevated temperatures, a weak T_g signal in the range of 213–240°C was revealed in the as-spray-formed composite. Furthermore, the dimension shrinkage of the composite was only 0.5% during the TMA test, which is much smaller than that of amorphous ribbon counterpart by up to 20%. The enhanced hardness by constituent second phases and the dimension stability of the composite are associated with their inherent microstructure, the primary crystals in particular.
[doi:10.2320/matertrans.MJ200767]

(Received November 30, 2006; Accepted March 15, 2007; Published June 20, 2007)

Keywords: *bulk metallic glass, $Al_{89}La_6Ni_5$, melt-spun ribbon, spray forming, hybrid composite*

1. Introduction

Aluminum rich-rare earth element-transition metal (Al-RE-TM) alloys have been intensively studied in the past decade.[1–7] The partially devitrified ribbons with strength over 1 GPa were regarded as a new class of composite materials, *nanophase composites*.[8] A nanometer scale dispersion of fcc-Al crystals in an amorphous matrix was the key feature of the microstructures. The microstructures were examined by an atom-probe field-ion microscopy[9] and the rare-earth component was demonstrated to pile up around the fcc-Al crystals due to inherently slow diffusing velocity. Kim *et al.*[10] has ascribed the hardening origin to the presence of small crystals that are defect free and capable of having a greater resistance to deformation than the amorphous matrix.

In spite that the nanophase composites have excellent performance, the studies up to now have been still limited to the ribbon dimension. Spray forming process[11–14] has been increasingly used to produce these composites in bulk dimension.[13–16] In this study, an as-spray-formed $Al_{89}La_6Ni_5$ nanophase composite[13] mixed together with 30% primary crystals (1 μm in diameter) was produced. In addition to the nanoscale fcc-Al crystals effect mentioned above, the primary crystals are another origin associated with the enhanced strength of the composite.

The purpose of this study was to produce glass matrix composite by spray forming process and elucidate the strengthening mechanisms of as-spray-formed $Al_{89}La_6Ni_5$ glass matrix composite in terms of the microstructure, nanoindentation and dynamic modulus measurement. The strength of corresponding as-melt-spun ribbons was also measured and served as a baseline for comparison.

*Corresponding author, E-mail: tsao_cya@mail.ncku.edu.tw

2. Experimental Method

A spray-formed $Al_{89}La_6Ni_5$ alloy plate was obtained with a thickness of 1–2 mm and a diameter of 200 mm (designated as LaSD). The preparation procedure was described elsewhere 13]. Some material was cut from the as-spray-formed plate and subsequently melt-spun into ribbons at wheel speeds of 15 m/s (designated as La15) and 30 m/s (designated as La30). Melt-spun ribbons were sectioned into 10 mm long pieces, glued into a sandwich-like body and then impregnated with epoxy resin in a vacuum chamber (Buehler), where the air pores adjacent to the specimens could be eliminated effectively and the interfaces between ribbons and resin maintained well. The excellent interfaces made it possible for the subsequent polishing steps to achieve a mirror surface without scratches. Extremely flat surfaces of the specimens were necessary for the accuracy of nanoindentation experiments.

Dynamic scanning calorimetry (Perkin Elmer pyris-1 DSC), dynamic mechanical analyzer (Perkin Elmer DMA) and thermal mechanical analyzer (Perkin Elmer TMA) were used for thermal and mechanical experiments. In a viscous solid, oscillatory stress is delayed from supplied oscillatory strain by viscosity at an angle of δ. Complex modulus is the ratio of the maximum stress to the maximum strain and the real and imaginary parts of the complex modulus were defined as storage (E') and loss (E'') modulus, respectively. E' is the value of the energy which was stored and recovered perfectly during one cycle of strain change, while E'' was the loss of energy which changed to heat during one cycle. The loss tangent ($\tan\delta$) corresponded to the internal friction representing the degree of heat which was lost during the test.[12,17] The heating rate for DSC was 0.67 K/s, but for DMA and TMA was 0.16 K/s. Nanoindentation tests were

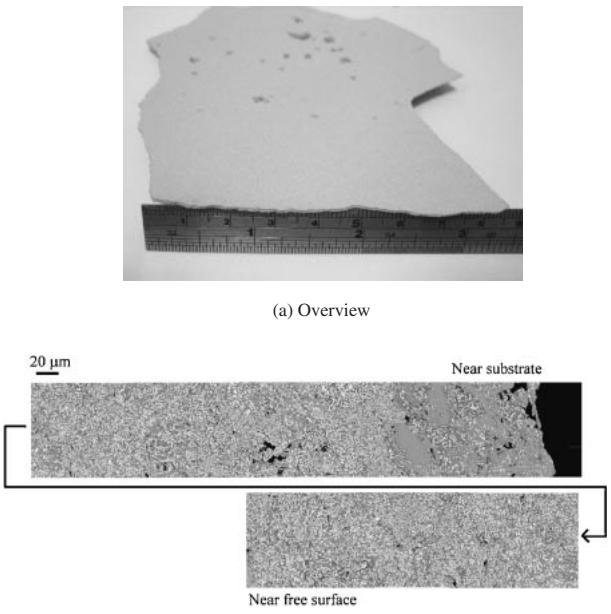

(a) Overview

(b) Cross-sectional

Fig. 1 (a) Overview and (b) cross-sectional micrographs of as-spray-formed $Al_{89}La_6Ni_5$ composite plate.

Table 1 Chemical compositions of various $Al_{89}La_6Ni_5$ specimens measured by wavelength-dispersive-spectrometry technique.

at%	LaSD (matrix)	La15	La30
Al	89.5 ± 2	87.5 ± 0.1	87.6 ± 0.2
Ni	5.8 ± 1	4.7 ± 0.2	4.9 ± 0.1
La	4.6 ± 1	7.7 ± 0.1	7.4 ± 0.1

performed on a MTS-XP facility at 0.05 L/s of strain rate and 2000 nm of indentation depth. The load for the microhardness test was 50 g.

3. Results and Discussion

3.1 XRD and DSC

At the end of the spray forming process, the deposit flew off from high-speed rotating ram and crashed into pieces. Figure 1 shows the overview and cross-sectional micrographs of a broken as-spray-formed LaSD deposit with about 1–2 mm in thickness. The cross-sectional micrograph, Fig. 1(b), exhibits the microstructure transition from near substrate to near free surface. More featureless areas, glassy phases, were formed near the substrate than near free surface because of the forced cooling effect from the substrate. A huge amount of primary crystals, 64 v/o, were also uniformly generated in addition to the glassy phases, which together can be considered as a metallic glass matrix composite. The chemical compositions of the LaSD matrix and the corresponding ribbon counterparts are listed in Table 1. The La depletion in the matrix of the LaSD specimen is due to precipitation of $Al_{11}La_3$ crystals.

Figure 2 shows the XRD results of LaSD, La15 and La30. The effects of the cooling rate are manifest clearly on the three materials. The La30 specimen with the highest cooling rate is mainly amorphous without showing any characteristic

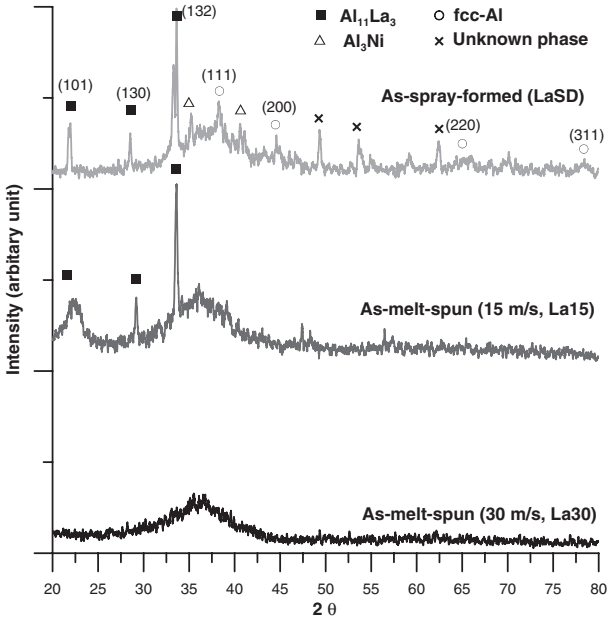

Fig. 2 XRD results of as-spray-formed and as-melt-spun $Al_{89}La_6Ni_5$ alloys.

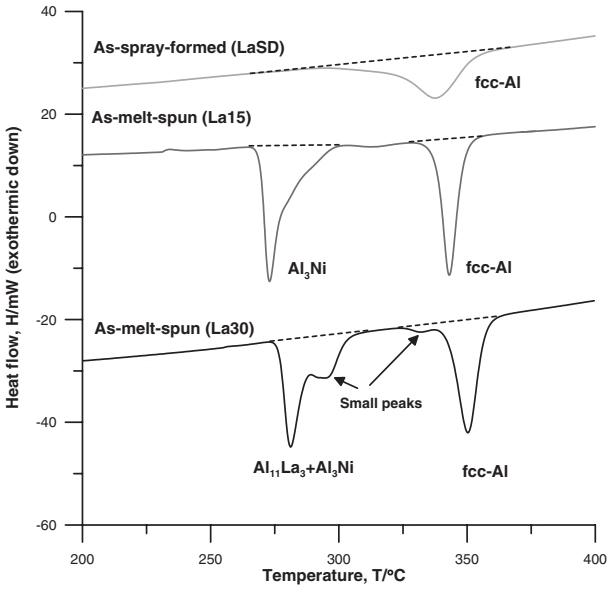

Fig. 3 DSC results of as-spray-formed and as-melt-spun $Al_{89}La_6Ni_5$ alloys.

peaks. The XRD of the La15 for a medium cooling rate is similar to that of the La30, except for a few characteristic peals. Therefore, the La15 is partially amorphous with crystal phases in the devitrified specimen, the largest amount of which was identified as $Al_{11}La_3$. The XRD of the LaSD specimen is also similar to that of the La30, except for a large amount of characteristic peaks. Due to the lowest cooling rate, the LaSD, although partially amorphous, has several crystal phases in the devitrified specimen, which were mainly identified as Al_3Ni and fcc-Al, and $Al_{11}La_3$.

DSC results further verify the XRD results as shown in Fig. 3. There is only one peak shown for the LaSD, which corresponds to the fcc-Al crystal phase. Since all the crystal phases has existed in the LaSD as shown in the XRD result,

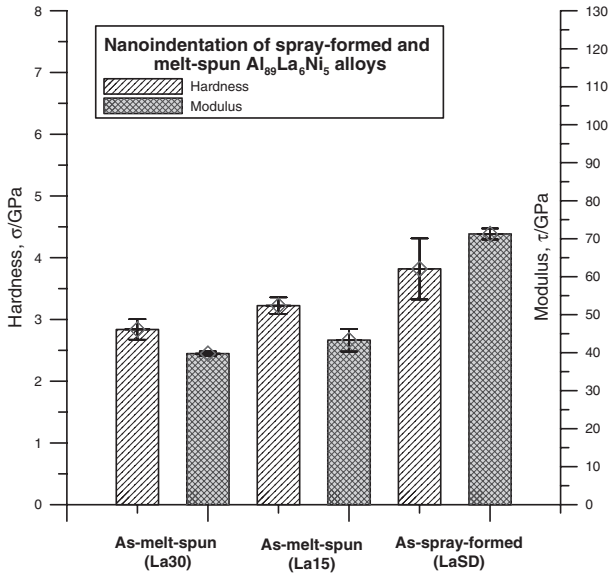

Fig. 4 Hardness and modulus of as-spray-formed and as-melt-spun $Al_{89}La_6Ni_5$ alloys obtained from nanoindentation tests.

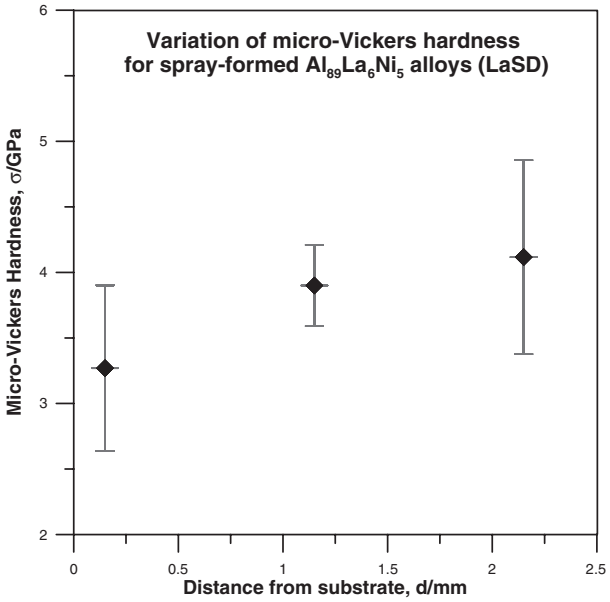

Fig. 5 Variations of microhardness in the cross-section of as-spray-formed $Al_{89}La_6Ni_5$ composite plate.

no exothermic peaks are shown in the DSC result. The exothermic peak indicates that the LaSD is partially amorphous, which devitrified during the DSC heating to form fcc-Al crystal phase. There are two distinct peaks for the La15, indicating two crystal phases were formed during the DSC heating. The La15 consists of amorphous matrix and $Al_{11}La_3$ crystal phase already as shown in the XRD result, and the two exothermic peaks shown in the DCS result correspond to the other two crystal phases, Al_3Ni and fcc-Al, which were formed during the DSC heating. There are three exothermic DSC peaks shown in the La30 with two of them overlapped with each other. As the La30 was originally fully amorphous, all the crystal phases, Al_3Ni, $Al_{11}La_3$ and fcc-Al, were formed during the DSC hearting. It is shown that the peaks of the former two overlap with each other.

3.2 Nanoindentation and microhardness

Hardness and modulus results of as-spray-formed (LaSD) and as-melt-spun specimens (La15 and La30) from nano-indentation tests are shown in Fig. 4. For the melt-spun specimens, as the wheel velocity decreases by 50% from La30 to La15, the hardness of the material increases by 14%. The modulus of the material also increases by 9%. It's attributed to the microstructure transition from '*amorphous*' of the La30 to '*amorphous plus $Al_{11}La_3$*' of the La15. The hardness was effectively increased by the crystal phases embedded in the amorphous matrix. The crystal phase ($Al_{11}La_3$) is therefore beneficial for the hardness and modulus of the materials.

For the spray-formed LaSD, the hardness significantly increases by 18% and the modulus greatly increases by 64%. The increase of the hardness is mainly due to the micro-structure changing from '*amorphous plus $Al_{11}La_3$*' for the La15 to '*amorphous plus primary crystals ($Al_{11}La_3$ + Al_3Ni) and secondary crystals (fcc-Al)*' for the LaSD. The strengthening effect comes from not only the μm-scale primary crystals, $Al_{11}La_3$ and Al_3Ni, in the LaSD, but the nm-scale secondary crystal, fcc-Al, in the amorphous matrix. The effects of the crystal phases on increasing the hardness were demonstrated again.

The hardness of the glass matrix composite is dependent on the volume % and hardness (and modulus) of constituent phases, as known as a mixture rule. That is, the hardness of the glass matrix composite increases with the increase in the amount of hard second phases. The hardness of pure amorphous material is shown as 3.1 GPa, which was obtained from the La30 specimen. The hardness of the primary crystals is taken as 5.1 GPa.[14] A LaSD composite consists of 36 v/o amorphous phase and up to 64 v/o crystals. As a result, the hardness of the overall glass matrix composite LaSD can be estimated to be 4.4 GPa ($0.36 \times 3.1 + 0.64 \times 5.1$). The calculated value agrees quite well with the hardness of LaSD shown in Fig. 4.

Micro-Vickers hardness tests were also performed on the LaSD specimen from near substrate to near free surface, as shown in Fig. 5. The cooling rate is the fastest for the material close to the substrate due to the fast heat extraction from the LN-cooled substrate. Therefore, the amount of amorphous phase is the largest and the amount of crystal phases is the smallest close to the substrate. Due to less crystal phase to inhibit the deformation, the hardness is smaller closer to the substrate. Hardness gradually increases from 3.2 GPa to 4.1 GPa as the distance from substrate increases.

The morphology of the microhardness indent on the LaSD specimen is shown in Fig. 6(a). The pile-up of local material around the pyramid-shape indent indicates that the LaSD material deformed via plastic deformation, which is the typical deformation mode of the crystallized materials. However, there are shear bands (marked by arrows) formed around the nanoindent of the La30, which is fully amorphous, as shown in Fig. 6(b). This is consistent with that the deformation mode of the amorphous materials is the propagation of the shear bands.

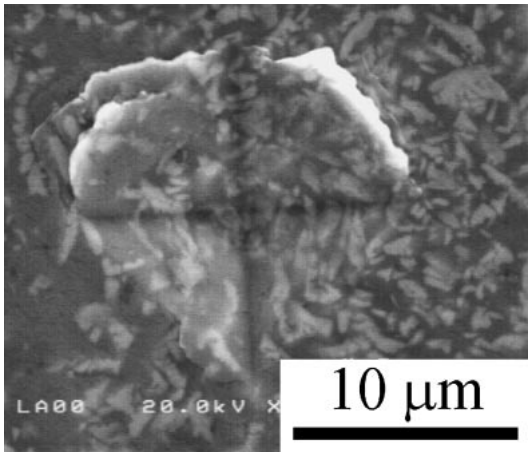

(a) LaSD

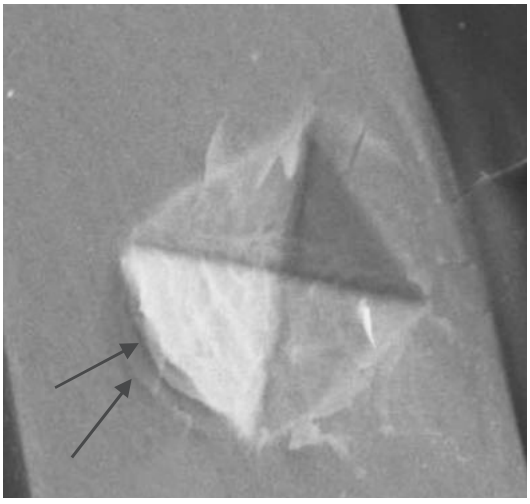

(b) La30

Fig. 6 Morphologies of indents on the (a) as-spray-formed and (b) as-melt-spun $Al_{89}La_6Ni_5$ alloys after microhardness tests.

3.3 Dynamic modulus

Figure 7 shows the variations of storage modulus (E') and loss modulus (E'') with temperature of the LaSD specimen as heated to 450°C at a vibration rate of 10 Hz obtained from the DMA test. The E' is generally proportional to the specimen strength and becomes smaller at higher temperature. The E' slightly decreases from 29.2 GPa at 104.7°C to 27.5 GPa at 240.5°C for the LaSD. But even the lowest E' value at 450°C is still over 20 GPa. The variations of the E'' mainly depends on the evolution of amorphous matrix during dynamic mechanical test. A glass transition behavior is indicated by the maximum E'' temperature observed around 241°C.

The LaSD specimen contains 36% glassy phase.[13] It is difficult to detect the glass transition temperature (T_g) from the DSC trace shown in Fig. 3 due to this low content of the amorphous phase. However, the glass-transition phenomenon was found in both the DMA and TMA tests. Figure 8 shows the results of TMA test from the LaSD as heated to 350°C. The glass-transition temperature is about 239°C from the TMA test, very close to the 241°C obtained from the DMA test.

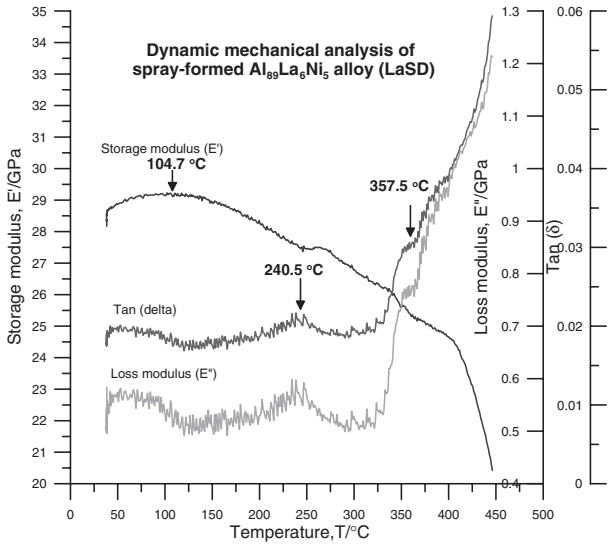

Fig. 7 Dynamic mechanical analysis of as-spray-formed $Al_{89}La_6Ni_5$ composite plate.

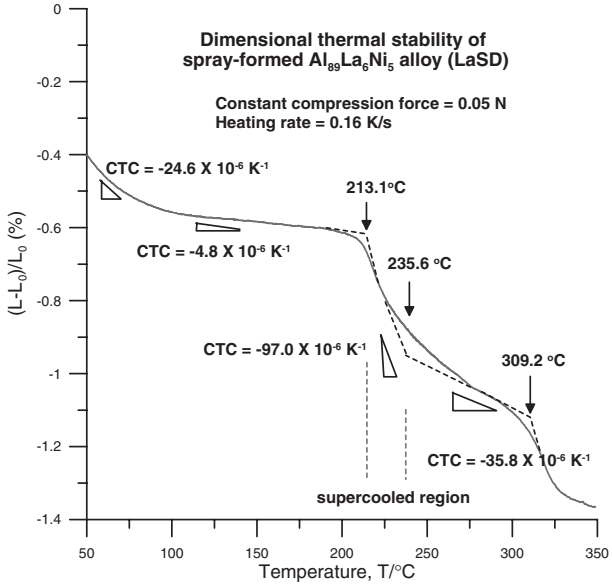

Fig. 8 Dimensional thermal stability of as-spray-formed $Al_{89}La_6Ni_5$ composite plate (LaSD).

3.4 Dimensional thermal stability

Before the crystallization of glass materials, small shrinkage due to structural relaxation occurs, which brings excess free volume to the equilibrium. Once the crystallization starts, large shrinkage is generated due to atomic rearrangement. At the same time, thermal expansion still occurs throughout these shrinkage events. Therefore, the result obtained by TMA is from the combination of the shrinkage and thermal expansion.

The dimensional thermal stability of LaSD specimen as heated to 350°C is also shown by Fig. 8. The LaSD, containing some amount of amorphous phase, shrinked less than 0.5%, and maintained excellent dimension stability even being heated up to 200°C. After heated over 200°C, a large shrinkage was observed near the supercooled liquid region, from 213.1°C to 235.6°C.

4. Conclusions

(1) A metallic glass matrix composite plate of $Al_{89}La_6Ni_5$ containing 36% amorphous phase with a thickness of 1–2 mm and a diameter of 200 mm was produced by spray forming process.
(2) Three main crystal phases, Al_3Ni, $Al_{11}La_3$ and fcc-Al, were found in the fully devitrified $Al_{89}La_6Ni_5$ material.
(3) The hardness of the spray-formed metallic glass composite obtained from nanoindentation increases by 18% and the modulus greatly increases by 64%, compared to the fully amorphous material, because the hardness was effectively increased by the crystal phases embedded in the matrix.
(4) The storage modulus, E', slightly decreases from 29.2 GPa at 104.7°C to 27.5 GPa at 240.5°C for the $Al_{89}La_6Ni_5$ metallic glass composite. The E' value at 450°C is still over 20 GPa.
(5) Tg of the $Al_{89}La_6Ni_5$ metallic glass composite obtained from the loss modulus and dimensional thermal stability curves is about 240°C.
(6) The LaSD, containing some amount of amorphous phase, shrinked less than 0.5%, and maintained excellent dimension stability even being heated up to 200°C.

Acknowledgement

The financial support from the National Science Council and Frontier Material and Micro/Nano Science and Technology Center, National Cheng Kung University, Tainan, Taiwan, is greatly appreciated.

REFERENCES

1) G. J. Shiflet, Y. He and S. J. Poon: J. Appl. Phys. **64** (1988) 6863.
2) L. C. Chen and F. Spaepen: Letter to Nature **336** (1988) 366.
3) A. Inoue, T. Zhang and T. Masumoto: Mater Trans. JIM **965** (1989) 972.
4) A. L. Greer: Science **267** (1994) 1947.
5) K. Lu: Mater. Sci. Eng. R **16** (1996) 161.
6) A. Inoue: Prog. Mater. Sci. **43** (1998) 365.
7) J. H. Perepezko, R. J. Hebert and W. S. Tong: Intermetallics **10** (2002) 34.
8) Z. C. Zhong, X. Y. Jiang and A. L. Greer: Mater. Sci. Eng. A **226–228** (1997) 531.
9) K. Hono, Y. Zhang and A. Tsai: Scripta metall. **32** (1995) 191.
10) Y. H. Kim, K. Hiraga, A. Inoue, T. Masumoto and H. H. Jo: Mater. Trans. JIM **35** (1994) 293.
11) Y. H. Su and C. Y. A. Tsao: Metall. Mater. Trans. **28B** (1997) 1249.
12) Y. M. Chen, Y. H. Su, R. W. Lin and C. Y. A. Tsao: Acta Mater. **46** (1998) 1011.
13) M. L. T. Guo, C. Y. A. Tsao, J. C. Huang and J. S. C. Jang: Mater. Sci. Eng. A **404** (2005) 49.
14) M. L. T. Guo, C. Y. A. Tsao, J. C. Huang and J. S. C. Jang: Intermetallics **14** (2006) 1069.
15) C. R. M. Afonso, C. Bolfarini, C. S. Kiminami, N. D. Bassim, M. J. Kaufman, M. F. Amateau, T. J. Eden and J. M. Galbraith: Scripta Mater. **44** (2001) 1625.
16) C. R. M. Afonso, C. Bolfarini, C. S. Kiminami, N. D. Bassim, M. J. Kaufman, M. F. Amateau, T. J. Eden and J. M. Galbraith: J. Non-Cryst Solid **284** (2001) 134.
17) H. Okumura, A. Inoue and T. Masumoto: Mater. Trans. JIM **32** (1991) 593.